Editors' Suggestion | Featured in Physics

Super Interferometric Range Resolution

John C. Howell,[1,2,*] Andrew N. Jordan,[1,2,4] Barbara Šoda,[5] and Achim Kempf[5]
[1]Institute for Quantum Studies, Chapman University, Orange, California 92866, USA
[2]Racah Institute of Physics, The Hebrew University of Jerusalem, Jerusalem, Israel, 91904
[3]Center for Coherence and Quantum Optics, University of Rochester, Rochester, New York 14627, USA
[4]Department of Physics and Astronomy, University of Rochester, Rochester, New York 14627, USA
[5]Department of Applied Mathematics and Department of Physics, University of Waterloo, and Perimeter Institute for Theoretical Physics, Waterloo, Ontario, Canada

(Received 7 March 2023; accepted 13 June 2023; published 2 August 2023)

We probe the fundamental underpinnings of range resolution in coherent remote sensing. We use a novel class of self-referential interference functions to show that we can greatly improve upon currently accepted bounds for range resolution. We consider the range resolution problem from the perspective of single-parameter estimation of amplitude versus the traditional temporally resolved paradigm. We define two figures of merit: (i) the minimum resolvable distance between two depths and (ii) for temporally subresolved peaks, the depth resolution between the objects. We experimentally demonstrate that our system can resolve two depths greater than 100× the inverse bandwidth and measure the distance between two objects to approximately 20 μm (35 000 times smaller than the Rayleigh-resolved limit) for temporally subresolved objects using frequencies less than 120 MHz radio waves.

DOI: 10.1103/PhysRevLett.131.053803

Range resolution [1–6] is the ability to determine the distance between two objects along the same line-of-sight when performing remote sensing. The prevailing thought is that radar range resolution is inextricably linked to the inverse bandwidth of a pulse [5,6] or to the wavelength of the electromagnetic wave owing to the coherent nature of the interfering wavefronts. We quote, "Wave theory indicates that the best vertical resolution that can be achieved is one-quarter of the dominant wavelength [7]. Within that vertical distance any reflections will interfere in a constructive manner and result in a single, observed reflection" [8]. The desire for better range resolution has driven scientists and engineers to ever-higher frequencies for radar and lidar [9–12]. However, this comes at a severe cost because transmission through and reflection from various material media is critically tied to frequency [8,13–16]. We dramatically improve upon these widely accepted limits of range resolution using a novel class of self-referenced functions to demonstrate several orders of magnitude improvement in range resolution beyond known limits.

For transform-limited pulses, two radar targets are considered range resolved when the range resolution distance d_r obeys the inequality

$$d_r \geq \frac{c\tau}{2}, \tag{1}$$

where c is the speed of light, τ is the pulse width, and 2 comes from the round-trip of the pulse [5,6]. Phase or frequency encoding are commonly employed to realize high time-bandwidth product pulses, which when

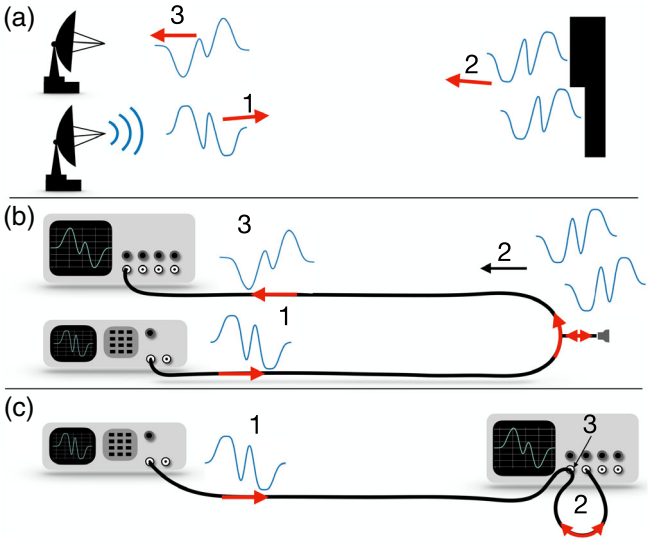

FIG. 1. Free-space (a) and guided-wave (b) and (c) ranging experimental schematics. Using parameter estimation techniques on interference-class waveforms, we estimate the distance between two scattering depths from a target which would otherwise be temporally subresolved.

combined with match-filtered pulse compression, lead to high temporal resolution. Therefore, a more general range resolution for a pulse is set by the inverse bandwidth [5,6]. Going beyond these limits has been historically difficult. Wong and Elefthiardes used superoscillations to reduce ranging uncertainty by 36% [17]. Recently, Komissarov *et al.* used partially coherent radar in an attempt to decouple range resolution from the signal bandwidth [18] achieving a factor of 10 improvement. We classify the current state of the art as a "temporally resolved" paradigm.

Here, we introduce a new "amplitude resolved" paradigm using self-referenced interference-class functions as shown in Fig. 1. An interference-class pulse is sent to a remote object. Multiple scattering depths along the same line of sight result in the interference of temporally shifted versions of the waveform. The resultant waveform is measured by the receiver. In theory, by using parameter estimation, we can determine range, distance between objects, relative scattering amplitudes, etc. We expect that amplitude-resolution ranging methods have been unexplored because of the inability to distinguish between loss and subresolved interference peaks.

Our system relies on parameter estimation from the interference between coherent pulses. A fundamentally different parameter estimation has also been used to overcome the spatial Rayleigh resolution limit of incoherent sources using mode sorting [19–23], allowing for fundamental definitions of spatial resolution [24–26]. Of note, Ansari *et al* used two incoherent optical pulses and mode decomposition to achieve supertemporal resolution [27].

In designing our functions, we employ two behaviors. First, a region of the function must be very sensitive to interference requiring extended and steep temporal gradients. Second, a zero-gradient region within the function, which is insensitive to the interference, is used as an amplitude reference. In this manner, as long as all portions of the pulse experience the same attenuation (or amplification) and there is a flat spectral response in a medium or upon reflection, the range resolution properties of the pulse are preserved.

We consider three types of pulse functions as shown in Fig. 2(a). The dashed orange line shows a specially designed interference-class, bandlimited pulse. The second interference class function is shown in solid green line, which we denoted as a "triangle" function. The dotted blue line shows a standard sinc^2 pulse, which is not an interference-class function, but is only used as a means of comparison of a Rayleigh criterion for temporal pulse resolution. The bandlimit for the sinc^2 and the custom function, in the image is the same. The corresponding fast Fourier transforms are shown in Fig. 2(b).

For the first type of self-referenced pulses, we use bandlimited function theory (e.g., used in superoscillations [28–32]) to generate our specially designed functions. While it is likely that similar behavior could be achieved

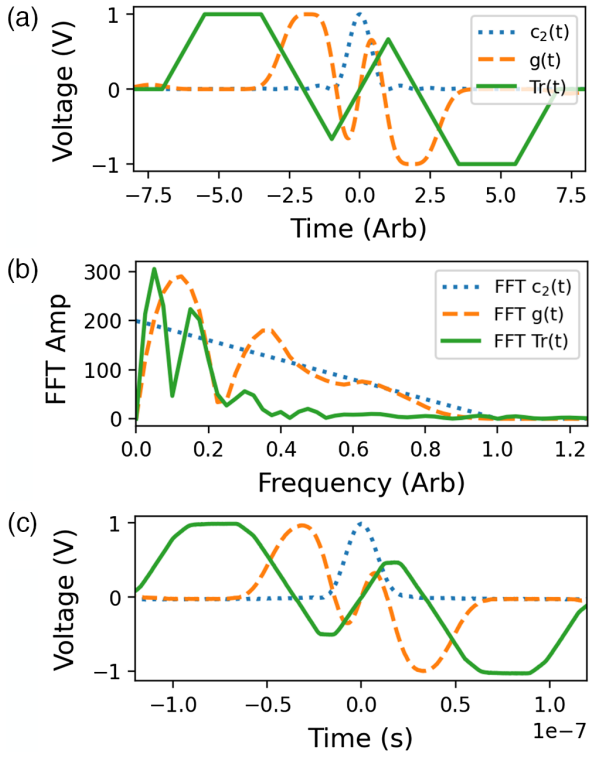

FIG. 2. Pulses and fast Fourier transforms. Panel (a) shows the functions used in the Letter. Panel (b) shows their Fourier transforms. Panel (c) shows the interfered waveforms from the coherent interference of two equal-amplitude pulses.

with many different types bandlimited functions, we use the formalism of Šoda and Kempf [32]. We generate our tailored and bandlimited functions by exploiting the product of a bandlimited "canvas" $c(t)$ function and arbitrary (e.g., Taylor) polynomials $f_n(t)$:

$$g(t) \coloneqq f_n(t)c_m(t), \tag{2}$$

where we use

$$c_m(t) = \mathrm{sinc}\left(\frac{\Omega t}{m}\right)^m \tag{3}$$

and

$$f_n(t) = \sum_{k=0}^{n-1} a_k t^k. \tag{4}$$

For $m > n$ this is a square-integrable function with bandlimit set by Ω. See Supplemental Material for more information [33]. We note that the specific polynomial function used herein is not unique—more generalized, optimized functions that have the features we describe here will be pursued in future work.

For the second type of self-referenced functions, we introduce an idealized line-segment function we call a

"triangle pulse" $\mathrm{Tr}(t)$, shown in solid green in Fig. 2(a). The triangle pulse is not bandlimited, so we consider approximations to the bandwidth based on the Fourier transform. Nevertheless, this function is better for measuring the minimum distance between two objects (range resolved objects) owing to the linearity of S over the full interference range.

Our third type of function is not an interference-class function, but is used simply to define a temporally resolved function. Similar to the Rayleigh criterion [34], when the peak of one pulse is separated by a distance greater than first minimum of a second pulse, the pulses are considered to be resolved. A classic example is the sinc^2,

$$c_2(t) = \mathrm{sinc}\left(\frac{\Omega t}{2}\right)^2. \tag{5}$$

For a bandlimited pulse, the minimally Rayleigh-resolved temporal shift t_R (the time analog of resolvability in space) is given by $t_R = 2\pi/\Omega$. How deeply we can superresolve the targets is quantified by the ratio

$$r_s = t_d/t_R, \tag{6}$$

where t_d is the temporal delay between the two returning pulses. Since r_s is both a function of the delay t_d and the bandwidth $t_R = 2\pi/\Omega$, for the work herein it is more precise to change the bandlimit to test the fundamental properties of the relative shift in the system rather than changing the relative pulse delay.

We define a signal S akin to balanced interferometric detection used to measure transverse deflections [35], namely,

$$S = \frac{A_{\mathrm{cmax}} - A_{\mathrm{cmin}}}{A_{\mathrm{lmax}} - A_{\mathrm{lmin}}}, \tag{7}$$

where A_{cmax}, A_{cmin} are the maximum and minimum amplitude of the function in the steep center region, respectively and A_{lmax}, A_{lmin} are the maximum and minimum of the flat temporal lobes.

Consider the ranging experiments shown in Fig. 1. In Fig. 1(a), waveforms are sent to a two-depth target. Upon reflection, the two reflected waveforms interfere and are sent to the receiver. The resultant waveform is measured and processed to estimate the distance between the two depths of the target.

To better test the limits of this technique, we use low-noise guided-wave experiments as shown in panels 1(b) and 1(c). Figure 1(b) shows a guided-wave equivalent to the free-space radar. However, there are unequal amplitudes from the scattered waves measured at the receiver based on the splitting ratios of the tee junction. To create equal-amplitude interference, we used the experiment shown in Fig. 2(c), which is the radio wave equivalent of the Michelson interferometer. In Fig. 1(c), the delay cable is connected to both channels 1 and 2. Channel 1 measures the interfered waveform and channel 2 measures the input (non-interfered) waveform. Both input channels on the scope are set at 1 MΩ to achieve the desired reflections and measurement. The experiments in Figs. 2(b) and 2(c) utilize high precision frequency tunability to achieve ultrasmall relative pulse shifts r_s.

The functions are generated numerically, consisting of 4000 points and a duration of 40 t_R units. These signals were uploaded to an arbitrary waveform generator (AWG). The bandlimit of the system is set by the repetition rate of the arbitrary waveform generator. For example, a repetition rate of 1 MHz results in a 40 MHz bandlimit for the bandlimited pulses.

To perform the ranging experiments as shown in Fig. 1(c), the arbitrary waveform generator sends the signal down the cable. The $g(t)$ pulse is sent to channel 1 of the oscilloscope and is teed to another cable which then adds a one-way temporal measured delay of $t_c = 4.4$ ns (the measured delay is 3.8 ns when not connected to channel 2 and the measured cable length is $l_c = 72$ cm) implying that the pulse delay is $t_d = 2t_c = 8.8$ ns. The reflected signal from channel 2 interferes in channel 1 with the original displaced signal the $g(t)$ function. When using the bandlimited function $g(t)$, for example, channel 1 then measures $g(t) + g(t + 2t_c)$ and similarly for the other functions.

Figure 2(c) shows the resultant interference waveform in channel 1 for the three different types of pulses used herein for $t_s = 0.5t_R$. There are several important features of this graph that should be noted. First, the $c_2(t)$ interference pattern is not resolved, as expected, since $t_s = 0.5t_R$. Second, the interference regions in the center of the $g(t)$ (peaks have changed value) and triangle functions $\mathrm{Tr}(t)$ (interference plateaus) have changed dramatically. Third, the heights of the side lobes are still roughly constant for both interference-class functions.

We consider two important figures of merit for this range resolution system: (i) the minimum distance to amplitude-resolve two objects and (ii) the distance resolution between objects when the objects are amplitude resolved but still temporally subresolved (i.e., $r_s < 1$).

The triangle function is designed to amplitude resolve two objects with depths that are closely spaced along the same line of sight. Typically, in radar, the spectral bandwidth is given by the width of the spectrum at the 3 dB down point. However, owing to the irregular spectrum of the triangle pulse we use a conservative estimate based on where most of the power is found. Using the bandwidth from the Fourier transform as shown in Fig. 2(b), we can see that most of the power lies below 20% of the bandlimit for the bandlimited functions using the same pulse repetition rate. As noted above, the bandlimited frequency was 40× the repetition rate. From this observation, we define a

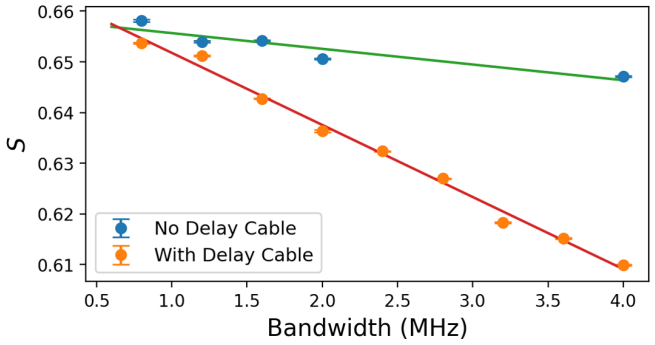

FIG. 3. The signal S is plotted against bandwidth of the triangle function with (interference) and without (no interference) a delay cable.

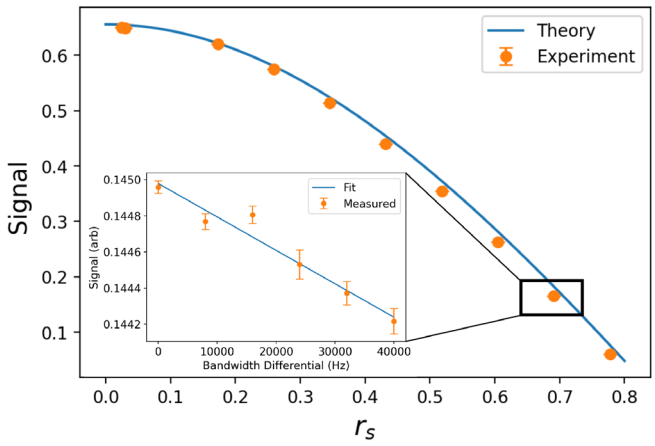

FIG. 4. Signal S vs time shift. The signal S from Eq. (7) is computed and measured as a function of the relative shift of two $g(t)$ functions.

conservative bandwidth of the triangle function to be 8× the pulse repetition rate.

The resolving power of the triangle function can be determined from Fig. 3. Here, we used the 72 cm delay cable disconnected from channel 2 and only connected to channel 1 yielding a 7.6 ns round-trip delay time. We change the bandwidth of the triangle pulse until we can no longer distinguish between the S curve with and without a cable. Here, we see that at approximately 1 MHz bandwidth, it is possible to distinguish the signal with and without the delay cable. This corresponds to $r_s \approx 0.008$ or better than 100 times the inverse bandwidth.

To further demonstrate the power of this technique, we removed the 72 cm cable and used only the extra path length of a bnc T junction, which has about 1.3 cm path length. We used a 2.5 GSa/s triangle function with 10 samples per time unit t_R (401 total points as opposed to 4000 described above) and measured the interference signal on an 800 MHz oscilloscope. The estimated bandwidth of the signal, based on the Fourier transform, was approximately 100 MHz, but with some small amount of frequency content up to 500 MHz. With and without the T junction, the value of S was 0.5573 ± 0.0002 and 0.5511 ± 0.0004, respectively, or a separation of 15 standard deviations. This implies sub-mm resolution. We then added a male-to-male bnc connector that added another couple centimeters and the value dropped to 0.5285 ± 0.0001.

The second important figure of merit for range resolution is the ability to determine the distance between two objects for temporally subresolved pulses. Figure 4 shows the signal S vs r_s (the ratio of the round-trip cable delay to the Rayleigh criterion) using the bandlimited function $g(t)$. It can be seen in Fig. 4 that the theory and experiment agree well.

The slope of S tells us the sensitivity of the system to changes in the relative temporal shift of the two functions. The S function for the bandlimited pulse is roughly quadratic in the region of zero shift and becomes linear after about $r_s = 0.5$ or half the Rayleigh resolved time. We want to know how well this system can determine the relative time between two shifts r_{s1} and r_{s2}. For a fixed cable length,

$$\Delta r_s = 2t_c \frac{\Delta\Omega}{2\pi}, \tag{8}$$

where $\Delta r_s = r_{s2} - r_{s1}$ and $\Delta\Omega/2\pi$ is the smallest resolvable change in the bandwidth of the pulse.

In the inset of Fig. 4, it shows the change in the signal of a small incremental frequency shift. Using the 72 cm cable with $t_c = 4.4$ ns delay and a 2 MHz repetition rate ($\Omega/2\pi = 80$ MHz bandlimit) resulted in approximately $t_s = 0.69$ shift. The bandwidth of the pulses was changed from 79.960 to 80 MHz in increments of 8.0 kHz. Each trace was averaged 512 times and each setting was measured 10 times with 15 to 30 sec between each measurement. Assuming a signal to noise ratio of 1, we can resolve 80 MHz bandwidth changes down to about 3.2 kHz. These data imply $\Delta r_s = 2.8 \times 10^{-5}$. The inferred depth resolution of our system is then $\Delta x = v_c t_R \Delta r_s/2 \approx$ 20 μm. Thus, for a target with two equal-amplitude, temporally subresolved reflected pulses, we can measure the relative distance between them down to 35 000 times below the Rayleigh limit and several orders of magnitude below the timing resolution of the oscilloscope.

While the primary emphasis of this paper concerns the simplest case of equal-amplitude reflections like those obtained using the setup in Fig. 1(c), in realistic applications, target reflection amplitude will typically be unequal, like those generated in Fig. 1(b). In the Supplemental Material [33], we show a two-parameter signal that involves both a temporal shift and disparate amplitudes and disparate amplitudes based.

We note several important comments. (i) These experiments were done using low frequency radio wavelengths. However, they are equally valid in all parts of the electromagnetic spectrum. (ii) As demonstrated preliminarily, the

system can be generalized to account for disparate reflection amplitudes and multiple layers by creating more exotic functions and signal analysis. (iii) It is straightforward to convert time resolution to space resolution by transversely scanning the receiver in Fig. 1(a) and solving the inverse problem opening up high resolution imaging.

In summary, we have demonstrated both theoretically and experimentally that it is possible to obtain range resolution far better than the Rayleigh criterion or the inverse bandwidth. We employed the coherent aspects of radio wave transmission and detection to measure sensitive interference patterns. In the future work, we will explore the fundamental limits of this technique, as well as apply this method to more realistic ranging tasks in the field.

J. C. H. and A. N. J. acknowledge support from Chapman University and the Bill Hannon Foundation. A. K. acknowledges support through a Discovery Grant of the National Science and Engineering Council of Canada (NSERC), a Discovery Project grant of the Australian Research Council (ARC) and a Google Faculty Research Award. B. S. is supported by the Perimeter Institute, which is supported in part by the Government of Canada through the Department of Innovation, Science and Economic Development Canada and by the Province of Ontario through the Ministry of Economic Development, Job Creation and Trade.

*johhowell@chapman.edu

[1] Donald R. Wehner, *High Resolution Radar* (Artech House, Inc., Norwood, MA, 1987), p. 484.
[2] Jian Li, Guoqing Liu, Nanzhi Jiang, and Petre Stoica, Moving target feature extraction for airborne high-range resolution phased-array radar, IEEE Trans. Signal Process. **49**, 277 (2001).
[3] K. B. Cooper, R. J. Dengler, G. Chattopadhyay, E. Schlecht, J. Gill, A. Skalare, I. Mehdi, and P. H. Siegel, A high-resolution imaging radar at 580 GHz, IEEE Microwave Wireless Compon. Lett. **18**, 64 (2008).
[4] Fangzheng Zhang, Qingshui Guo, and Shilong Pan, Photonics-based real-time ultra-high-range-resolution radar with broadband signal generation and processing, Sci. Rep. **7**, 13848 (2017).
[5] Merrill Ivan Skolnik, *Introduction to Radar Systems* (McGraw Hill Book Co., New York, 1980), p. 590.
[6] Nadav Levanon and Eli Mozeson, *Radar Signals* (John Wiley & Sons, New York, 2004).
[7] Robert E. Sheriff, Seismic Stratigraphy—Applications to Hydrocarbon Exploration (American Association of Petroleum Geologists, 1977), 10.1306/M26490C1.
[8] Adrian Neal, Ground-penetrating radar and its use in sedimentology: Principles, problems and progress, Earth-Sci. Rev. **66**, 261 (2004).
[9] R. T. H. Collis, Lidar, Appl. Opt. **9**, 1782 (1970).
[10] Ulla Wandinger, *Introduction to Lidar* (Springer, New York, 2005).
[11] Xiaoye Liu, Airborne lidar for dem generation: Some critical issues, Prog. Phys. Geogr. **32**, 31 (2008).
[12] Behnam Behroozpour, Phillip A. M. Sandborn, Ming C. Wu, and Bernhard E. Boser, Lidar system architectures and circuits, IEEE Commun. Mag. **55**, 135 (2017).
[13] Tomohiro Oguchi, Electromagnetic wave propagation and scattering in rain and other hydrometeors, Proc. IEEE **71**, 1029 (1983).
[14] Ahmed I. Al-Shamma'a, Andrew Shaw, and Saher Saman, Propagation of electromagnetic waves at MHz frequencies through seawater, IEEE Trans. Antennas Propag. **52**, 2843 (2004).
[15] Andrew Shaw, A. I. Al-Shamma'a, S. R. Wylie, and D. Toal, Experimental investigations of electromagnetic wave propagation in seawater, in *2006 European Microwave Conference* (IEEE, 2006), pp. 572–575, 10.1109/EUMC.2006.281456.
[16] Shan Jiang and Stavros Georgakopoulos, Electromagnetic wave propagation into fresh water, J. Electromagn. Anal. Appl. **2011**, 261 (2011).
[17] Alex M. H. Wong and George V. Eleftheriades, Super-oscillatory radar imaging: Improving radar range resolution beyond fundamental bandwidth limitations, IEEE Microwave Wireless Compon. Lett. **22**, 147 (2012).
[18] Rony Komissarov, Vitali Kozlov, Dmitry Filonov, and Pavel Ginzburg, Partially coherent radar unties range resolution from bandwidth limitations, Nat. Commun. **10**, 1423 (2019).
[19] Mankei Tsang, Quantum Imaging beyond the Diffraction Limit by Optical Centroid Measurements, Phys. Rev. Lett. **102**, 253601 (2009).
[20] H. Shin, Kam Wai Clifford Chan, H. J. Chang, and R. W. Boyd, Quantum Spatial Superresolution by Optical Centroid Measurements, Phys. Rev. Lett. **107**, 083603 (2011).
[21] Mankei Tsang, Subdiffraction incoherent optical imaging via spatial-mode demultiplexing, New J. Phys. **19**, 023054 (2017).
[22] Weng-Kian Tham, Hugo Ferretti, and Aephraim M. Steinberg, Beating Rayleigh's Curse by Imaging Using Phase Information, Phys. Rev. Lett. **118**, 070801 (2017).
[23] Yiyu Zhou, Jing Yang, Jeremy D. Hassett, Seyed Mohammad Hashemi Rafsanjani, Mohammad Mirhosseini, A. Nick Vamivakas, Andrew N. Jordan, Zhimin Shi, and Robert W. Boyd, Quantum-limited estimation of the axial separation of two incoherent point sources, Optica **6**, 534 (2019).
[24] Mikael P. Backlund, Yoav Shechtman, and Ronald L. Walsworth, Fundamental Precision Bounds for Three-Dimensional Optical Localization Microscopy with Poisson Statistics, Phys. Rev. Lett. **121**, 023904 (2018).
[25] Carmine Napoli, Samanta Piano, Richard Leach, Gerardo Adesso, and Tommaso Tufarelli, Towards Superresolution Surface Metrology: Quantum Estimation of Angular and Axial Separations, Phys. Rev. Lett. **122**, 140505 (2019).
[26] J. Řeháček, M. Paúr, B. Stoklasa, D. Koutný, Z. Hradil, and L. L. Sánchez-Soto, Intensity-Based Axial Localization at the Quantum Limit, Phys. Rev. Lett. **123**, 193601 (2019).
[27] V. Ansari, B. Brecht, J. Gil-Lopez, J. M. Donohue, J. Řeháček, Z. Hradil, L. L. Sánchez-Soto, and C. Silberhorn,

Achieving the ultimate quantum timing resolution, PRX Quantum **2**, 010301 (2021).

[28] Y. Aharonov, S. Popescu, and D. Rohrlich, How can an infra-red photon behave as a gamma ray, Tel-Aviv University Preprint TAUP, 1847–1890 (1990).

[29] Michael V. Berry, Optical currents, J. Opt. A **11**, 094001 (2009).

[30] Sacha Kocsis, Boris Braverman, Sylvain Ravets, Martin J. Stevens, Richard P. Mirin, L. Krister Shalm, and Aephraim M. Steinberg, Observing the average trajectories of single photons in a two-slit interferometer, Science **332**, 1170 (2011).

[31] Konstantin Y. Bliokh, Aleksandr Y. Bekshaev, Abraham G. Kofman, and Franco Nori, Photon trajectories, anomalous velocities and weak measurements: A classical interpretation, New J. Phys. **15**, 073022 (2013).

[32] Barbara Šoda and Achim Kempf, Efficient method to create superoscillations with generic target behavior, Quantum Stud. Math. Found. **7**, 347 (2020).

[33] See Supplemental Material at http://link.aps.org/supplemental/10.1103/PhysRevLett.131.053803 for additional information and calculations about bandlimited functions, the Rayleigh criterion, signal analysis and multi-parameter estimation.

[34] Max Born and Emil Wolf, *Principles of Optics: Electromagnetic Theory of Propagation, Interference and Diffraction of Light* (Elsevier, New York, 2013).

[35] P. B. Dixon, D. J. Starling, A. N. Jordan, and J. C. Howell, Ultrasensitive Beam Deflection Measurement via Interferometric Weak Value Amplification, Phys. Rev. Lett. **102**, 173601 (2009).